Check for updates

American Journal of Hematology

WILEY

RESEARCH ARTICLE OPEN ACCESS

Therapeutic Silencing of Tmprss6 Reduces Iron-Induced Inflammation and Prolongs Survival in MDS Mice

Shahla Vilcassim[1,2] | Nuttanan Pholngam[1,3,4] | Rattanawan Thubthed[1,5,6] | Tiwaporn Nualkaew[1,7] | Saovaros Svasti[4] | Pornthip Chaichompoo[5] | Kai Kysenius[8] | Peter J. Crouch[8] | Sibylle Dames[9] | Mona Eisermann[9] | Alberto Martinez[10] | Ute Schaeper[9] | Jim Vadolas[1,11] | George Grigoriadis[1]

[1]Centre of Cancer Research, Hudson Institute of Medical Research, Melbourne, Victoria, Australia | [2]School of Clinical Sciences at Monash Health, Monash University, Clayton, Victoria, Australia | [3]Graduate Program in Molecular Medicine, Faculty of Science, Mahidol University, Bangkok, Thailand | [4]Thalassemia Research Center, Institute of Molecular Biosciences, Mahidol University, Nakhon Pathom, Thailand | [5]Department of Pathobiology, Faculty of Science, Mahidol University, Bangkok, Thailand | [6]Faculty of Medicine, Praboromarajchanok Institute, Ministry of Public Health, Nonthaburi, Thailand | [7]Department of Medical Technology, Walailak University, Nakhon Si Thammarat, Thailand | [8]Department of Anatomy & Physiology and Centre for Muscle Research, The University of Melbourne, Melbourne, Victoria, Australia | [9]Silence Therapeutics GmbH, Berlin, Germany | [10]Silence Therapeutics PLC, London, UK | [11]Department of Molecular and Translational Sciences, Monash University, Clayton, Victoria, Australia

Correspondence: Jim Vadolas (jim.vadolas@hudson.org.au)

Received: 6 October 2025 | **Revised:** 26 April 2026 | **Accepted:** 11 May 2026

Keywords: disease-modifying therapy | GalNAc-conjugated siRNA | hepcidin | iron overload | myelodysplastic syndromes | TMPRSS6

ABSTRACT

Myelodysplastic syndromes (MDS) are a heterogeneous group of clonal hematopoietic disorders characterized by ineffective hematopoiesis, cytopenias, and an increased risk of progression to acute myeloid leukemia (AML). Despite advances in supportive and targeted therapies, disease-modifying interventions remain limited. Iron overload is increasingly recognized as a key driver of disease progression, amplifying oxidative stress and inflammation while impairing hematopoietic function. However, the mechanisms by which sustained iron excess contributes to disease evolution remain poorly understood. Hepcidin, the master regulator of systemic iron homeostasis, is produced by hepatocytes in response to iron and inflammatory cues and is negatively regulated by transmembrane protease serine 6 (TMPRSS6). Targeting TMPRSS6 to increase endogenous hepcidin offers a promising strategy to restrict iron overload and its inflammatory consequences. Here, we investigated hepatocyte-targeted silencing of *Tmprss6* using a GalNAc-conjugated siRNA (SLN124) in the NUP98–HOXD13 (NHD13) mouse model of MDS. MDS and wild-type mice received monthly subcutaneous SLN124 (3 mg/kg) or oral deferiprone (1.25 mg/mL). Iron burden in MDS mice strongly correlated with ASC-speck formation in $CD45^+$ hematopoietic cells, consistent with inflammasome activation. Both SLN124 and deferiprone reduced tissue iron deposition and ASC-speck abundance, with SLN124 producing the most pronounced effect. Long-term SLN124 treatment delayed disease progression and significantly prolonged survival, with 30% of treated mice surviving beyond 450 days compared with complete mortality by Day 420 in controls and deferiprone-treated mice. These findings demonstrate that *Tmprss6* inhibition via SLN124 suppresses iron-driven inflammation, and mitigated disease progression in MDS mice, establishing TMPRSS6 silencing as a promising disease-modifying therapeutic approach.

Jim Vadolas and George Grigoriadis contributed equally to this work and share senior authorship.

This is an open access article under the terms of the Creative Commons Attribution-NonCommercial License, which permits use, distribution and reproduction in any medium, provided the original work is properly cited and is not used for commercial purposes.

© 2026 Silence Therapeutics GmbH and The Author(s). *American Journal of Hematology* published by Wiley Periodicals LLC.

1 | Introduction

Myelodysplastic syndromes (MDS) comprise a heterogeneous group of clonal hematopoietic stem and progenitor cell disorders characterized by ineffective hematopoiesis, dysplasia, and a risk of progression to acute myeloid leukemia (AML) [1]. Anemia represents the most prevalent and clinically debilitating feature of MDS and frequently necessitates recurrent red blood cell transfusions. While transfusion support provides symptomatic relief, it results in cumulative iron loading and significantly compromises quality of life [2–4]. Ineffective erythropoiesis in MDS expands immature erythroid precursors with high proliferative activity and iron requirements. To meet this demand, erythroid cells suppress hepatic hepcidin synthesis, thereby enhancing systemic iron availability through increased intestinal absorption [5]. Combined with transfusion-derived iron, this response leads to progressive tissue iron overload and excessive generation of reactive oxygen species (ROS). Oxidative stress induces genotoxicity, clonal instability, and further impairs erythropoiesis, while elevated ROS amplify inflammation, establishing a vicious cycle of oxidative and inflammatory damage that progressively undermines hematopoietic integrity [4, 6–8].

Recent studies have linked aberrant activation of the NLRP3 inflammasome and the emergence of clonal hematopoiesis of indeterminate potential (CHIP) to disease progression in MDS [9–11]. Upon activation, the inflammasome promotes cleavage of the pro-caspase-1 into active caspase-1, which converts pro-IL-1β and pro-IL-18 into mature cytokines [12]. This process leads to pyroptotic cell death and amplification of inflammatory signaling creating a chronically inflamed bone marrow microenvironment, that promotes ineffective hematopoiesis and clonal expansion. Inflammasome activation is accompanied by assembly of supramolecular complexes incorporating the adaptor protein ASC (apoptosis-associated speck-like protein containing a caspase recruitment domain), with ASC specks serving as biomarkers of the inflammatory milieu in MDS [13–15]. Moreover, the extracellular release of ASC specks from pyroptotic cells can further propagate inflammation, underscoring the broad impact of inflammasome activation on disease progression [16, 17].

Importantly, excess iron acts as a potent amplifier of oxidative stress and ROS generation, both of which are well-established activators of innate immune signaling and NLRP3 inflammasome activation [18]. In this context, the clinical significance of iron-mediated toxicity in MDS is supported by evidence linking both transfusion-independent and transfusion-acquired iron overload to accelerated disease progression in patients and animal models [2, 19–21]. Targeting iron metabolism, through chelation therapy has been shown to restore clonogenic potential in MDS-derived hematopoietic stem and progenitor cells (HSPCs), reduces oxidative DNA damage, and suppresses pro-inflammatory signaling, partly via NF-κB inhibition [3, 8, 22]. These effects align with clinical observations demonstrating improved hematopoietic parameters, reduced transfusion burden, and enhanced survival in MDS patients receiving chelation therapy [23–25]. Such findings highlight the potential of iron-directed interventions to modulate disease trajectory and improve clinical outcomes in MDS [4, 21].

Hepcidin, encoded by *Hamp*, is a liver-derived peptide hormone that regulates systemic iron homeostasis by binding and degrading the iron exporter ferroportin, thereby limiting dietary absorption and iron release from macrophages and hepatocytes [5]. Hepcidin expression is tightly regulated by the bone morphogenetic protein (BMP)/SMAD signaling whereas the transmembrane serine protease matriptase-2 (*Tmprss6*) acts as a negative regulator by cleaving hemojuvelin, a BMP co-receptor [5]. Targeting the TMPRSS6-hepcidin axis therefore provides a rational strategy to mitigate iron-mediated inflammation and disrupt the pathogenic cycle of MDS [26, 27].

In this study, we employed a liver-targeted GalNAc-conjugated siRNA (SLN124) to downregulate *Tmprss6* in hepatocytes [28–30]. In the NUP98-HOXD13 (NHD13) transgenic mouse model of MDS, which recapitulates key features of ineffective hematopoiesis and disease evolution, we evaluated the effects of sustained iron restriction across progressive disease stages [31]. Iron overload in the hematopoietic niche was most pronounced during early disease and was associated with increased ASC speck formation, a hallmark of inflammasome assembly in $CD45^+$ cells. Most notably, SLN124 not only enhanced endogenous hepcidin expression and promoted iron redistribution, but also significantly suppressed iron-driven inflammation and mitigated disease progression in MDS mice. These findings provide mechanistic insight into the role of iron-induced inflammation in MDS and establish proof-of-concept for TMPRSS6 inhibition as a potential disease-modifying strategy.

2 | Materials and Methods

2.1 | Treatment of MDS Mice

MDS mice were bred on a C57BL/6 background, housed under a constant light–dark cycle, and maintained on a standard commercial diet containing 200 ppm iron (Specialty Feeds, Glen Forrest, WA, Australia) with ad libitum access to food and water. For short-term studies, treatment commenced at 4 months of age and continued for 60 days. Both female and male mice were included. Mice received two doses of SLN124 (3 mg/kg) or control treatments: nontargeting siRNA (CTRL) or vehicle (phosphate-buffered saline, PBS), administered s.c. on Days 1 and 28. For long-term studies, treatment commenced at 6 months of age and continued until study endpoint, with siRNAs administered monthly via s.c. injections. PBS-treated controls were phenotypically indistinguishable from completely untreated mice across hematological and survival endpoints and therefore served as the reference comparator across treatment arms. The oral iron chelator DFP was supplied in drinking water at a concentration of 1.25 mg/mL for the duration of the study.

2.2 | Oligonucleotides

The oligonucleotides employed have been previously described and utilized in both murine and human studies [28–30]. SLN124 comprises a double-stranded 19-mer RNA oligonucleotide, modified with 2′-O-methyl, 2′-fluoro-2′-deoxy substitutions and

10968652, 0, Downloaded from https://onlinelibrary.wiley.com/doi/10.1002/ajh.70391 by Alberto Martinez - NICE, National Institute for Health and Care Excellence , Wiley Online Library on [08/06/2026]. See the Terms and Conditions (https://onlinelibrary.wiley.com/terms-and-conditions) on Wiley Online Library for rules of use; OA articles are governed by the applicable Creative Commons License

phosphorothioate bonds, targeting *Tmprss6*, which is conjugated to a tri-antennary GalNAc unit at the 5′ end of the sense strand. The control, CTRL, contains the same GalNAc ligand and siRNA modifications but uses an siRNA sequence directed against luciferase.

2.3 | Gene Expression Analysis

Approximately 10 mg of liver tissue was disrupted and homogenized in a Mixer Mill MM 400 (Retsch GmbH, Haan, Germany) using tungsten carbide beads (Qiagen, Hilden, Germany) and total RNA was prepared with InviTrap Spin Tissue RNA Mini Kit (Stratec, Berlin, Germany) according to the manufacturer's instructions (InviTrap Protocol). In all, 100 ng total RNA was used for real-time quantitative polymerase chain reaction (RT-qPCR) with amplicon sets/sequences for *Tmprss6*, hepcidin antimicrobial peptide (*Hamp*), and *Actin* (mACTB) (Eurogentec, Seraing, Belgium), respectively (Table S1). The RT-qPCR reactions were carried out with a QuantStudio 6 Flex (Applied Biosystems part of Thermo Fisher Scientific Inc., Waltham, MA, USA) using Takyon One-Step Low Rox Probe 5X MasterMix dTTP (Eurogentec). The data were calculated by using the comparative C_T method, also known as the $2^{-\Delta\Delta Ct}$ method.

2.4 | Hepcidin Assay

Serum hepcidin was quantified using the "Hepcidin Murine-Compete ELISA Kit" (Intrinsic Lifesciences, La Jolla, CA, USA) according to manufacturer's instructions.

2.5 | Serum Iron Studies

Serum iron and total iron binding capacity (TIBC) were determined using Beckman Coulter Analyzer at Monash Medical Centre, Melbourne. Transferrin saturation was calculated using the formula: Iron sat % = Fe/(transferrin × 25) × 100.

2.6 | Full Blood Examination

Blood was collected from the submandibular vein in heparinized tubes. Full blood examination (FBE) was performed using an automated Roche Applied Science Cobas Helios hematological analyzer at the Walter and Eliza Hall Institute, Melbourne, Australia.

2.7 | Immunofluorescence Staining

Bone and spleen tissues were fixed in 4% neutral-buffered formalin, before undergoing tissue processing and embedding in paraffin. Tissue sections were cut at a thickness of 4 μm using a Microm HM330 microtome and mounted onto Superfrost glass slides. Tissue sections were labeled with anti-mouse ASC (1:200, AG-25B-0006-C100, AdipoGen, San Diego, CA) and Rat anti-mouse CD45 (550539, BD Pharmingen, San Diego, CA), followed by staining secondary antibodies: donkey anti-rabbit Alexa Fluor 555 (A-31572, Thermo Fisher Scientific, United States) and donkey anti-rat Alexa 647 (712-605-153, Jackson ImmunoResearch, PA, United States), and nuclei visualized with DAPI. Fluorescence images were scanned and captured using Olympus VS120 scanner at UPLSAPO 20X objective lens and Nikon C1 confocal microscope at 60X oil objective lens. Details can be found in Supplemental Materials and Methods in Supporting Information.

2.8 | Quantitative Image Analysis

Perls' Prussian blue and immunofluorescence-stained BM and spleen sections were performed with the HALO image analysis platform for quantification and spatial analysis of (1) Perls' Prussian blue area, (2) CD45, and (3) ASC positive cells. Details can be found in the Supplemental Materials and Methods in Supporting Information. Schematic diagrams illustrating the methodology behind the analysis strategy can be found in Supplemental Methods Figures 1 and 2 in Supporting Information.

2.9 | Tissue Elemental Analysis

Elemental analysis of tissue samples was performed using laser ablation inductively coupled plasma mass spectrometry (LA-ICP-MS) for spatial mapping, and bulk quantification was conducted using inductively coupled plasma mass spectrometry (ICP-MS). Detailed methodologies for both techniques are provided in Supplementary Methods 3 and 4 in Supporting Information.

2.10 | Evaluation of Erythroid Differentiation in BM and Spleen at Endpoint

Erythroid cells were analyzed from the BM and spleen by flow cytometry using fluorescein isothiocyanate (FITC)-conjugated anti mouse-CD71, allophycocyanin (APC)-conjugated anti-mouse Ter119 and phycoerythrin (PE)-conjugated anti-mouse CD44 antibodies (BD Biosciences). This assay allows the separation of erythroid cells into distinct populations corresponding to (i) proerythroblasts, (ii) basophilic, (iii) polychromatic, (iv) reticulocytes, and (v) RBCs. For all the cytometric analyses, 7-amino-actinomycin D (7-AAD) was used as a viability dye, and immunophenotyping was carried out on 7-AAD^{-ve} cells. A minimum of 10 000 events were recorded for erythrocytes in BM and spleen. For all the analyses, cells were acquired using the LSR Fortessa X-20 using FACSDiva software (BD Biosciences), and the results were analyzed with FlowJo software (Tree Star Inc.).

2.11 | Statistical Analyses

All statistical analyses were conducted using GraphPad Prism Version 10 (GraphPad Software Inc., San Diego, CA, USA). Experimental data are presented as box plots or stacked bar charts. The statistical significance of differences between group

10968652, 0, Downloaded from https://onlinelibrary.wiley.com/doi/10.1002/ajh.70391 by Alberto Martinez - NICE, National Institute for Health and Care Excellence , Wiley Online Library on [08/06/2026]. See the Terms and Conditions (https://onlinelibrary.wiley.com/terms-and-conditions) on Wiley Online Library for rules of use; OA articles are governed by the applicable Creative Commons License

means was assessed using a two-tailed Student's *t*-test or ordinary one-way ANOVA, followed by Bonferroni's post hoc test. A *p*-value of less than 0.05 was considered statistically significant.

3 | Results

3.1 | MDS Mice Exhibit Significant Iron Overload in the BM and Spleen

MDS transgenic mice express the NUP98-HOXD13 fusion gene under the control of the Vav1 promoter, leading to the development of an MDS phenotype with progressive peripheral blood cytopenias and multilineage dysplasia. These mice display a protracted disease course, with transformation to acute leukemia typically occurring from 10 months of age, and do not survive beyond 14 months [31]. The extended latency suggests that additional molecular or environmental factors are required to drive leukemic progression. Prior studies have reported iron overload in MDS mice, implicating iron dysregulation as a potential contributor to disease evolution [21]. To explore this, we performed Perls' Prussian blue staining on BM and spleen sections from 6-month-old MDS mice. This revealed tissue iron accumulation in both BM and spleen, consistent with an iron overload phenotype and the model's suitability for iron restriction studies (Figure 1A,B).

To map the spatial distribution of metal ions in situ, we conducted LA-ICP-MS on BM and spleen from WT and MDS mice. Because copper, manganese, and zinc are essential cofactors for antioxidant enzymes such as superoxide dismutases and catalase, imbalances in these elements can modulate oxidative stress, inflammatory signaling, and hematopoietic function [32–35]. Measuring these metals enabled us to exclude their contribution to the inflammatory phenotype and confirm that the changes observed were specific to iron dysregulation. While copper, manganese, and zinc levels were comparable between WT and MDS tissues, iron concentrations were significantly elevated throughout the BM and spleen of MDS mice (Figure 1C,D). These data demonstrate a selective disruption of iron homeostasis in this MDS model and strengthen the mechanistic association between iron overload and disease.

3.2 | MDS Mice Displayed Distinct Patterns of ASC Speck Formation in CD45$^+$ Cells

Dysregulation of the innate immune system has been reported in MDS patients and is further supported by evidence of increased inflammasome activity, a key driver of inflammation [9, 10]. Central to inflammasome activation is the formation of ASC specks, which act as scaffolds for caspase-1 activation and the subsequent release of pro-inflammatory cytokines [13]. Owing to their distinct size and morphology (~1 μm), ASC specks can be readily detected by immunofluorescence microscopy, providing a robust, quantifiable readout of inflammasome activity. To assess inflammasome activity in the MDS model, we performed immunofluorescence staining for ASC specks in the BM and spleen of 6-month-old MDS and WT mice. Compared to WT controls, MDS mice exhibited a significant increase in ASC speck formation, predominantly within CD45$^+$ cells (Figure 2A–F). ASC specks were detected in both cytoplasmic and nuclear compartments. The observed speck size distribution was consistent with previous reports in human MDS, supporting the translational relevance of this model [13]. These findings indicate that inflammasome activation is an early pathological feature in MDS and suggest that ASC specks may serve as a surrogate biomarker for innate immune activation in preclinical models.

3.3 | Iron Deposition Correlates With ASC Expression in 6-Month-Old MDS Mice

Iron overload is closely linked to inflammation, as elevated iron levels can stimulate pro-inflammatory signaling pathways and promote innate immune activation [36]. Conversely, chronic inflammation itself can disrupt systemic iron homeostasis, further exacerbating iron accumulation [37]. To investigate the relationship between iron overload and inflammasome activation in MDS, we performed Perls' Prussian blue staining to visualize tissue iron deposits, followed by immunofluorescent staining for ASC on consecutively sectioned BM and spleen tissues from 6-month-old MDS mice. A significant positive correlation was observed between tissue iron content and the abundance of ASC$^+$ CD45$^+$ hematopoietic cells in both the BM and spleen (Figure 2G,H). Moreover, quantitative analysis demonstrated a strong association between tissue iron levels and ASC expression, as assessed by MFI, further supporting a mechanistic link between iron overload and inflammasome activation in this MDS model. These findings suggest that iron accumulation contributes to the inflammatory phenotype in MDS and provide a rationale for therapeutic strategies aimed at restricting iron availability to attenuate inflammasome activity and disease progression.

3.4 | SLN124 Induces Hepcidin Expression and Reduces Serum Iron Levels During the Early Treatment Phase in MDS Mice

Given the central role of hepcidin in regulating systemic iron homeostasis, therapeutic inhibition of TMPRSS6 offers a rational strategy to enhance hepcidin production and mitigate iron overload and inflammation in MDS. SLN124 is a GalNAc-conjugated siRNA therapeutic specifically designed to silence TMPRSS6 expression and restore iron balance in disorders associated with pathological iron overload [28–30]. To evaluate the efficacy of SLN124 in vivo, 4-month-old WT and MDS mice were treated with SLN124 (3 mg/kg subcutaneously on Days 1 and 28), and outcomes were compared to a standard oral iron chelator, deferiprone (DFP; 1.25 mg/mL in drinking water), over a 60-day period. The selected SLN124 dosing regimen was previously validated in murine models of hereditary hemochromatosis and β-thalassemia [28, 30]. SLN124 treatment significantly reduced hepatic *Tmprss6* mRNA expression and was associated with sustained elevation of circulating hepcidin levels 28 days after the final injection (Figure 3A–C). These molecular changes translated into marked reductions in serum iron, indicating effective suppression of systemic iron availability (Figure 3D). In

10968652, 0, Downloaded from https://onlinelibrary.wiley.com/doi/10.1002/ajh.70391 by Alberto Martinez - NICE, National Institute for Health and Care Excellence , Wiley Online Library on [08/06/2026]. See the Terms and Conditions (https://onlinelibrary.wiley.com/terms-and-conditions) on Wiley Online Library for rules of use; OA articles are governed by the applicable Creative Commons License

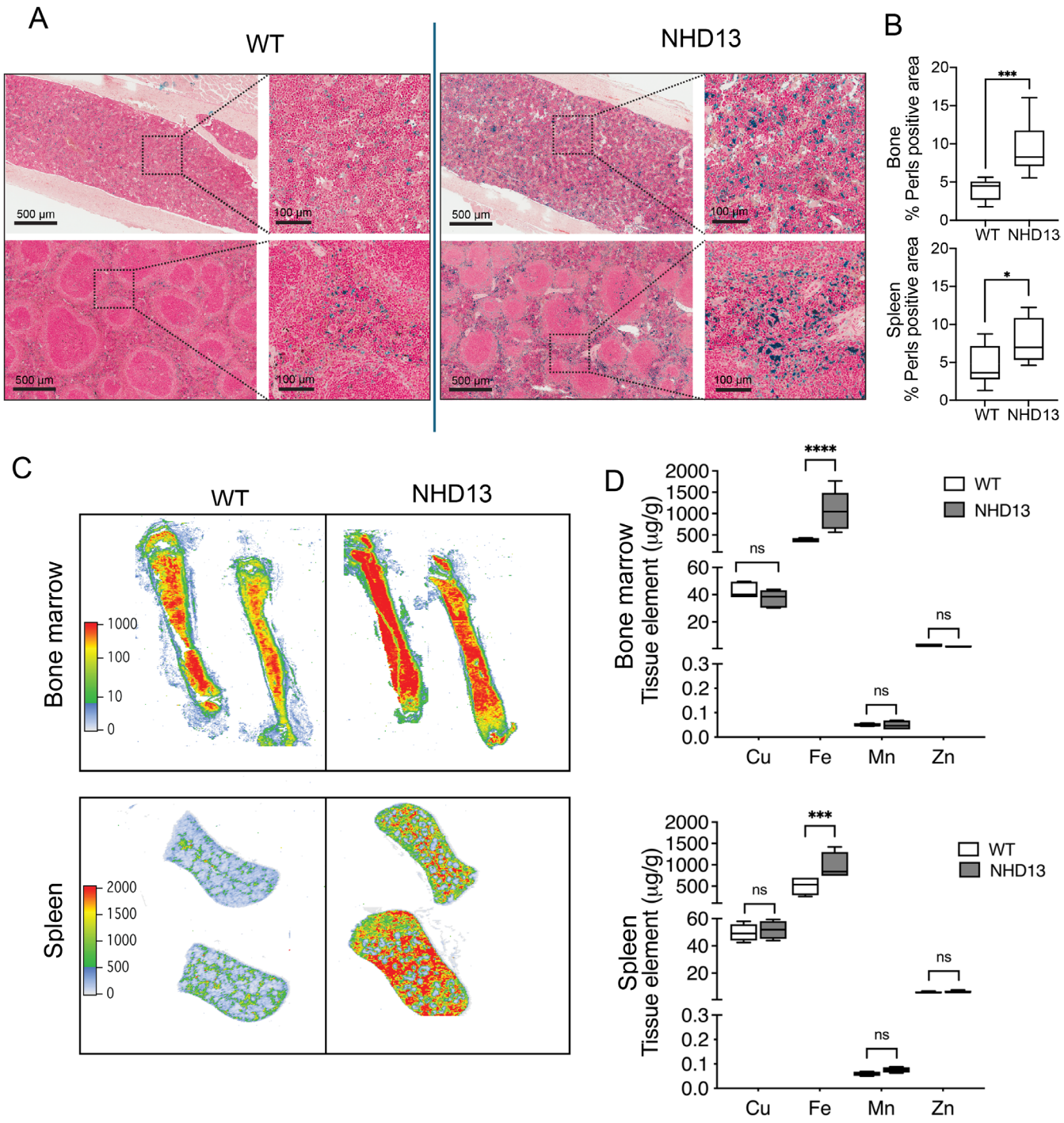


FIGURE 1 | Increased iron loading in the bone marrow and spleen of MDS mice. Bone marrow (BM) and spleens from 6-month-old WT and NHD13 mice were analyzed biochemically and histologically. (A) Representative Perls' Prussian blue–stained tissue sections showing iron distribution in BM and spleen. (B) Quantification of Perls' Prussian blue–positive area in BM and spleen sections. (C) Representative laser ablation–inductively coupled plasma–mass spectrometry (LA-ICP-MS) images of 10-µm tissue sections depicting anatomically defined iron distribution in BM and spleen of WT and NHD13 mice. (D) Quantification of Cu, Fe, Mn, and Zn levels (µg/g tissue) in BM and spleen determined by LA-ICP-MS. Results are shown as box plots ($n = 4–5$ mice/group). Data are presented as mean ± SEM. Statistical significance was determined using Student's *t*-test (ns, not significant; $^{*}p \leq 0.05$; $^{***}p \leq 0.001$; $^{****}p \leq 0.0001$).

contrast, DFP treatment alone did not alter *Tmprss6* or *Hamp* expression and failed to significantly impact serum iron parameters. These results demonstrate that SLN124 is a potent in vivo modulator of hepcidin expression and iron metabolism in the MDS model, supporting its therapeutic potential as a targeted strategy to correct iron dysregulation in MDS.

3.5 | Early SLN124 Treatment Modulates Erythroid Parameters in MDS Mice

We next evaluated the impact of iron restriction on erythropoiesis in MDS mice. At 6 months of age, MDS mice exhibited preserved erythropoietic function under steady-state conditions, as

10968652, 0, Downloaded from https://onlinelibrary.wiley.com/doi/10.1002/ajh.70391 by Alberto Martinez - NICE, National Institute for Health and Care Excellence , Wiley Online Library on [08/06/2026]. See the Terms and Conditions (https://onlinelibrary.wiley.com/terms-and-conditions) on Wiley Online Library for rules of use; OA articles are governed by the applicable Creative Commons License

reflected by normal levels of hemoglobin (Hb), hematocrit (Hct), and red blood cell (RBC) (Figure 3E–G). Despite these normal parameters, a notable increase in red cell distribution width (RDW) was observed, suggesting early erythroid dysregulation and the onset of disease progression (Figure 3H). A recent study reported alterations in RBC-related parameters in MDS mice as early as 6 months of age [21]. In our cohort overt erythropoietic dysregulation emerged after 6 months. This discrepancy likely reflects differences in disease staging and environmental conditions, including factors related to animal housing and diet composition, which can influence the timing of hematological manifestations.

Following SLN124 treatment, both WT and MDS mice exhibited comparable reductions in Hb levels relative to vehicle-treated controls, consistent with functional iron restriction. This reduction was accompanied by a significant decrease in Hct in WT mice, however, Hct remained stable in MDS mice, indicating

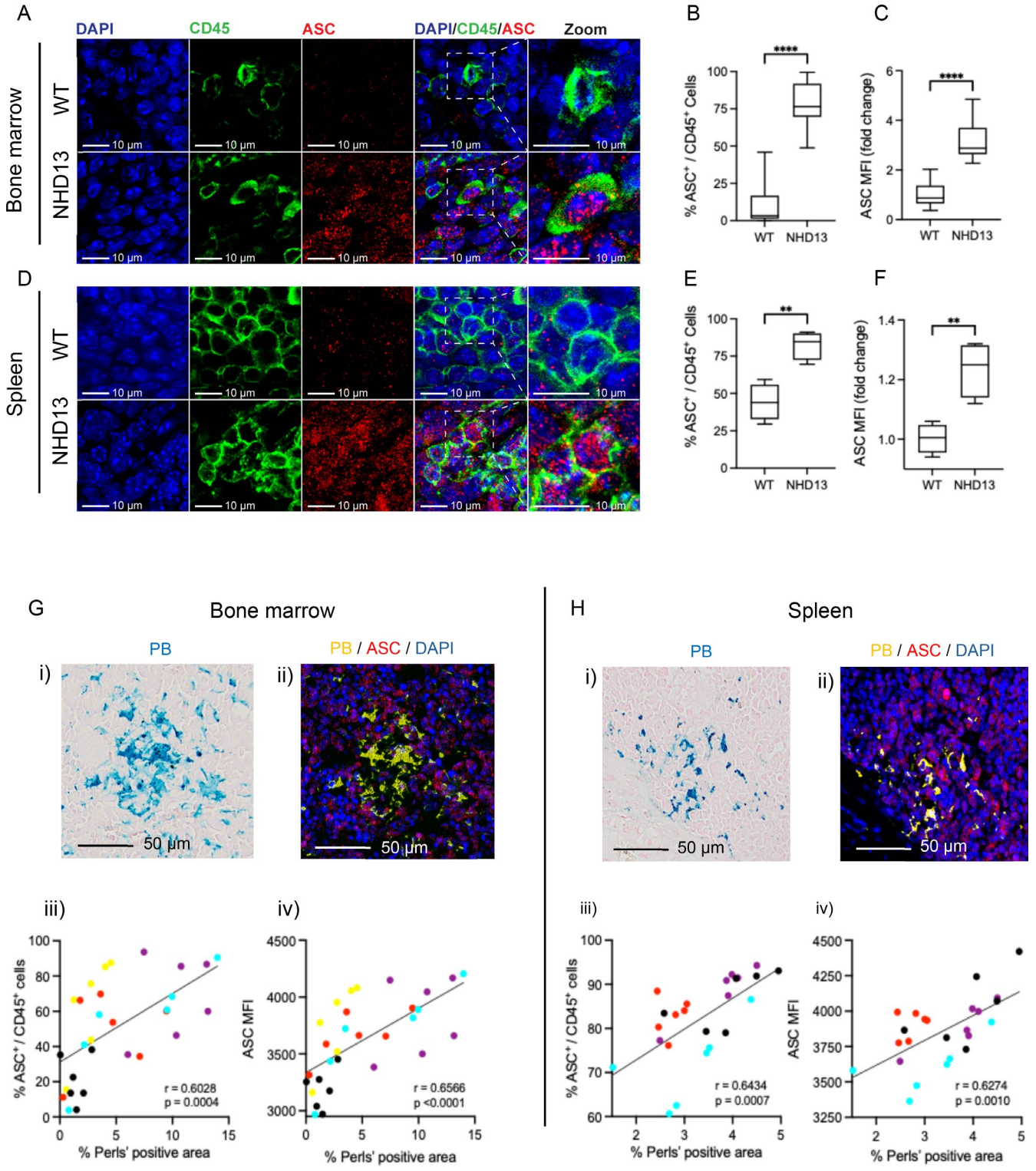


FIGURE 2 | Legend on next page.

10968652, 0, Downloaded from https://onlinelibrary.wiley.com/doi/10.1002/ajh.70391 by Alberto Martinez - NICE, National Institute for Health and Care Excellence , Wiley Online Library on [08/06/2026]. See the Terms and Conditions (https://onlinelibrary.wiley.com/terms-and-conditions) on Wiley Online Library for rules of use; OA articles are governed by the applicable Creative Commons License

FIGURE 2 | Increased ASC-speck expression correlates with iron deposition in presymptomatic MDS mice. BM and spleen samples from mice described in Figure 1 were analyzed by immunofluorescence. NHD13 mice showed pronounced ASC speck formation within $CD45^+$ hematopoietic cells in both BM (A–C) and spleen (D–F) compared with WT controls. Quantification includes the percentage of $CD45^+ASC^+$ double-positive cells (B, E) and ASC mean fluorescence intensity (MFI) fold change (C, F). Immunofluorescence staining included CD45 (green), ASC (red), and DAPI (blue). Consecutive tissue sections from mice described in Figure 1, were stained for iron and ASC to assess the relationship between ASC expression and iron deposition in the (G) BM and (H) spleen. Panels show (i) Perls' Prussian blue–stained areas, (ii) ASC immunofluorescence (red) with DAPI nuclei (blue) overlaid onto the corresponding iron-stained section with deconvoluted iron signal (yellow), (iii) correlation between $CD45^+ASC^+$ cells and Perls' Prussian blue–positive area, and (iv) correlation between ASC mean fluorescence intensity (MFI) and Perls' Prussian blue–positive area. Six iron-positive regions from BM and spleen were analyzed for ASC expression; colored circles indicate individual measurements from separate animals. Sections were analyzed using HALO software. Data are presented as box plots ($n = 4–5$/group). Statistical analysis was performed using Student's *t*-test (ns, not significant; $^*p \leq 0.05$; $^{**}p \leq 0.01$; $^{***}p \leq 0.001$; $^{****}p \leq 0.0001$). Spearman's correlation revealed a strong positive association between iron accumulation and ASC expression in both BM and spleen of NHD13 mice ($n = 4–5$/group).

a differential response to iron restriction. RDW values were unaffected by SLN124 treatment regardless of genotype in the short-term cohort. Notably, SLN124 administration resulted in a significant increase in reticulocyte counts in both WT and MDS mice, indicative of a compensatory erythropoietic response to reduced iron availability and impaired red blood cell maturation (Figure 3I).

Previous studies have reported the development of anemia in NHD13 mice by approximately 6 months of age. In our cohort, however, overt anemia was not consistently observed until 7–8 months, indicating a modest delay in phenotypic expression compared with earlier published studies [20, 21, 31, 38]. Mice in our study were maintained on standard chow containing > 200 ppm iron. Elevated dietary iron availability may partially support erythropoiesis and attenuate the development of overt anemia at earlier timepoints. Variation in dietary iron composition may influence the balance between systemic iron availability and inflammatory iron sequestration, thereby shifting the severity and timing of anemia onset. Higher iron availability can buffer hemoglobin levels and erythropoietic output, potentially delaying anemia at 6 months, whereas lower-iron diets may unmask earlier hematological deficits. These observations underscore the importance of dietary context when interpreting disease kinetics in iron-sensitive models. Furthermore, defining how the timing, intensity, and duration of iron modulation influence disease trajectory will be critical for identifying an optimal therapeutic window for clinical translation.

3.6 | Transient Iron Restriction Modulates Tissue Iron Distribution in MDS Mice

To evaluate the impact of SLN124 and DFP-mediated iron restriction on tissue iron loading, we examined BM and spleen sections from 6-month-old WT and MDS mice using Perls' Prussian blue staining to detect ferric (Fe^{3+}) hemosiderin deposits. Vehicle- and control siRNA-treated MDS mice demonstrated extensive, dense punctate staining in both BM and spleen, consistent with marked iron accumulation. In contrast, SLN124 or DFP treatment resulted in a visible reduction in Perls'-positive staining, particularly within the BM, where smaller and less intense hemosiderin deposits were observed (Figure 4A–C). This effect was less pronounced in the spleen, where iron deposition appeared relatively unchanged.

To complement these histological findings, total iron content in BM and spleen tissues was quantified by ICP-MS (Figures 4D,E and S3). While Perls' staining provides a qualitative assessment of localized ferric iron within defined anatomical compartments, particularly macrophage-rich regions where iron sequestration and recycling are actively regulated, ICP-MS quantifies total elemental iron in whole tissue homogenates, thereby averaging iron across all cellular components. Consequently, regional changes in iron deposition may be readily detected histologically yet appear modest when assessed by bulk elemental analysis. Taken together, these datasets are complementary rather than contradictory. The Perls' staining supports a reduction in localized pathological iron deposition, particularly within BM microenvironments enriched for erythroid–macrophage interactions, whereas ICP-MS indicates that overall tissue iron concentrations remain only modestly altered over the 60-day treatment period. These findings suggest that short-term iron modulation via TMPRSS6 inhibition or iron chelation does not substantially reduce total iron burden in BM or spleen but instead influences iron distribution and storage within specific cellular niches, with more pronounced microenvironmental effects observed in the BM.

We also provide evidence of altered Mn homeostasis following iron restriction therapy (Figure S3). Specifically, DFP-treated MDS mice exhibited a modest but statistically significant increase in hepatic Mn, with a similar trend observed in the spleen. States of iron deficiency are known to upregulate intestinal and cellular uptake of divalent metals, which may lead to secondary accumulation of Mn, Mg, and Zn in tissues [39]. Mn and Fe share overlapping regulatory and transport pathways, including flux mediated by divalent metal transporter 1 (DMT1; SLC11A2) and, to a lesser extent, ferroportin-dependent export [40]. Accordingly, iron chelation may enhance compensatory uptake or alter systemic distribution of Mn. Further mechanistic studies interrogating the role of DMT1 and related metal transport systems will be required to define the basis of altered Mn handling in this context. The physiological relevance of these modest changes in metal content remains to be determined.

3.7 | Iron Restriction Therapy Mitigates ASC-Speck Formation in MDS Mice

Given the critical role of iron in the progression of inflammation-related diseases, we hypothesized that targeting iron metabolism

10968652, 0, Downloaded from https://onlinelibrary.wiley.com/doi/10.1002/ajh.70391 by Alberto Martinez - NICE, National Institute for Health and Care Excellence , Wiley Online Library on [08/06/2026]. See the Terms and Conditions (https://onlinelibrary.wiley.com/terms-and-conditions) on Wiley Online Library for rules of use; OA articles are governed by the applicable Creative Commons License

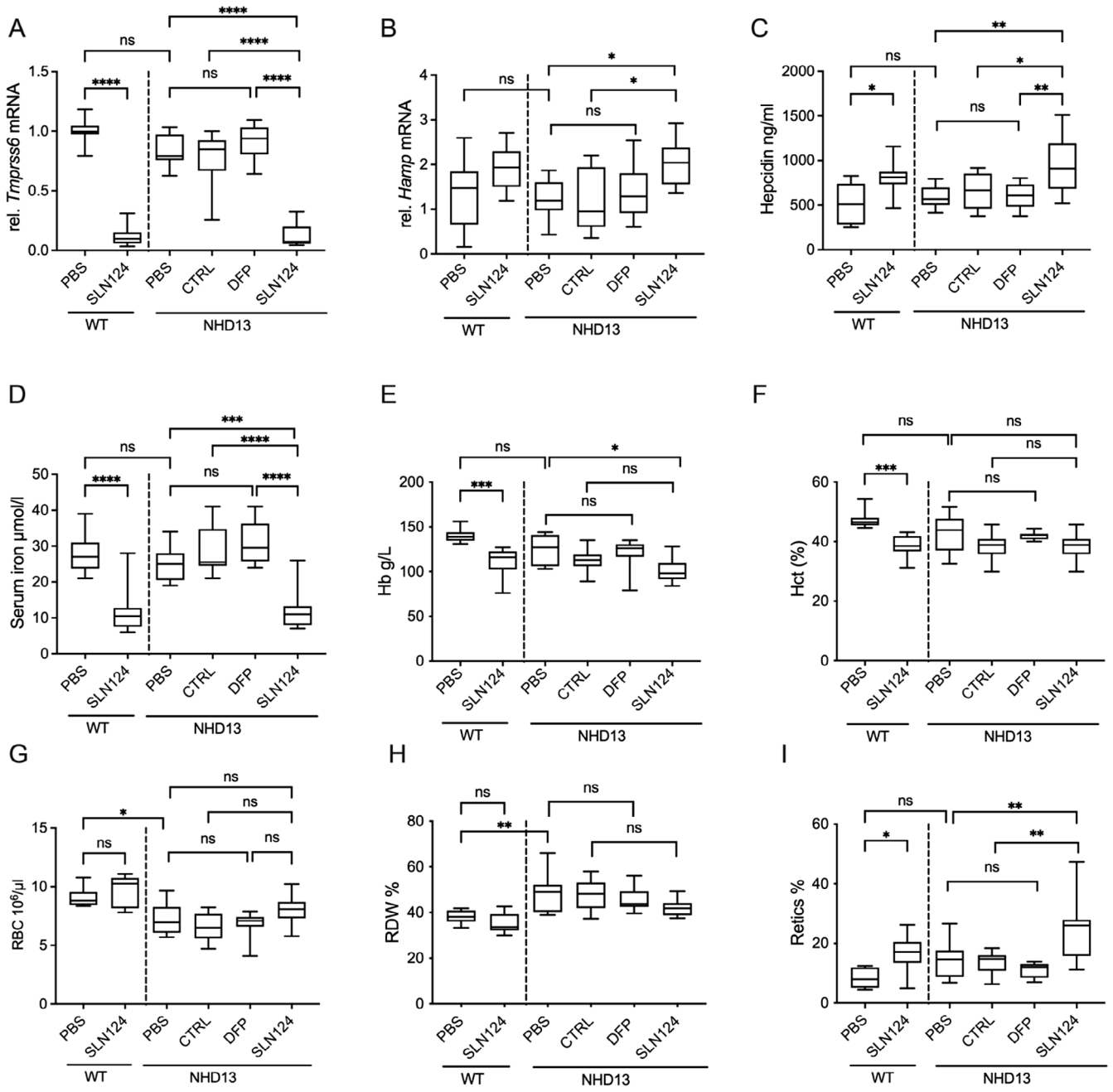


FIGURE 3 | SLN124 induces hepcidin, reduces serum iron, without reversing anemia in MDS mice. Four-month-old WT and NHD13 mice were treated with either SLN124 (3 mg/kg, two injections on Days 0 and 28) or DFP (administered in drinking water for 60 days). Control groups received vehicle (PBS) or non-target siRNA (CTRL). At experimental endpoint, mice were sacrificed and blood and tissues collected for hematological and biochemical analysis. (A) Hepatic *Tmprss6* mRNA; (B) hepatic *Hamp* mRNA; (C) serum hepcidin; (D) serum iron. *Tmprss6* and *Hamp* mRNA were quantified by RT-qPCR, normalized to β-actin, and expressed relative to NHD13 vehicle-treated controls (set at 1.0). Red blood cell parameters included: (E) hemoglobin (Hb); (F) hematocrit (Hct); (G) red blood cell counts (RBC); (H) red cell distribution width (RDW); (I) reticulocyte counts were measured 28 days after the final injection. Data are shown as box plots ($n = 8$–10/group). Statistical significance was assessed by one-way ANOVA with Bonferroni's post hoc test (ns, not significant; *$p \leq 0.05$; **$p \leq 0.01$; ***$p \leq 0.001$).

could attenuate inflammasome activation. ASC, which is normally found in both soluble cytoplasmic and nuclear forms, undergoes mobilization upon inflammasome assembly to form ASC specks (~1 µm in diameter). These structures serve as a robust and quantifiable marker of inflammasome engagement. To assess inflammasome activation in vivo, we performed high-resolution confocal microscopy and applied quantitative HALO image analysis to measure ASC speck formation in CD45$^+$ hematopoietic cells in the BM and spleen of 6-month-old WT and MDS mice following treatment with SLN124 or the iron chelator DFP. Both treatments significantly reduced ASC speck formation in CD45$^+$ cells within the BM relative to control-treated animals (Figure 5A,B). In contrast, only SLN124 treatment produced a significant reduction in ASC speck content within splenic CD45$^+$ cells compared with both DFP- and vehicle-treated MDS mice (Figure 5C–F). These findings indicate that

10968652, 0, Downloaded from https://onlinelibrary.wiley.com/doi/10.1002/ajh.70391 by Alberto Martinez - NICE, National Institute for Health and Care Excellence , Wiley Online Library on [08/06/2026]. See the Terms and Conditions (https://onlinelibrary.wiley.com/terms-and-conditions) on Wiley Online Library for rules of use; OA articles are governed by the applicable Creative Commons License

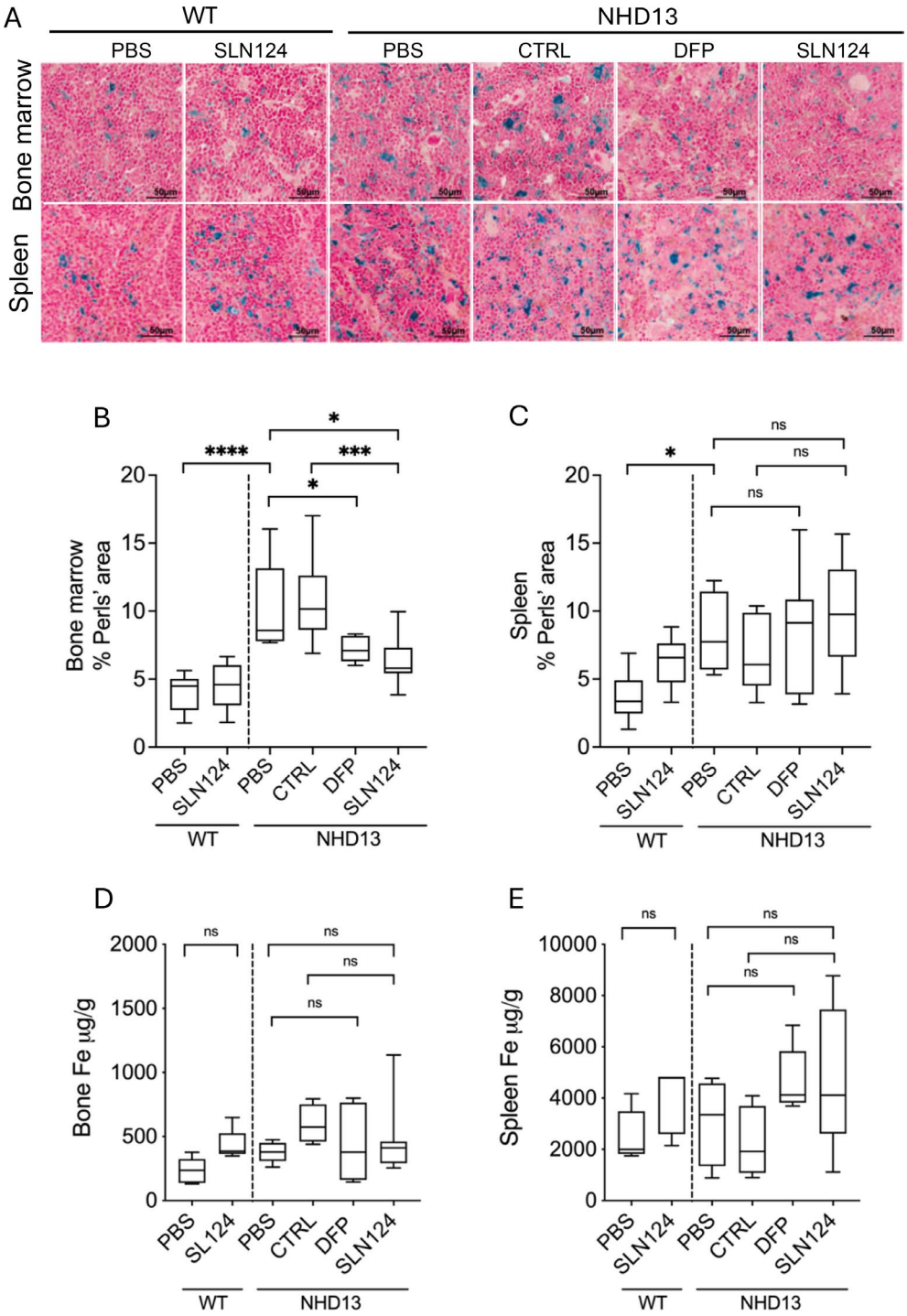


FIGURE 4 | Iron restriction therapy reduces tissue iron distribution in MDS mice. BM and spleen samples from mice described in Figure 3 were analyzed for iron content. (A) Representative Perls' Prussian blue–stained BM and spleen sections from WT and MDS mice. Quantification of Perls' Prussian blue–positive area in (B) BM and (C) spleen sections, measured 28 days after the final injection, for both treated and control groups. Note the reduction in Perls' Prussian blue–stain area in BM following SLN124 and DFP treatments. Results are presented as box plots ($n = 8$–10 mice/group). Inductively coupled plasma mass spectrometry (ICP-MS) was used to quantify iron content in (D) BM and (E) spleen from treated and control groups, with results shown as box plots ($n = 4$–5 mice/group). Statistical significance was determined by one-way ANOVA followed by Bonferroni's post hoc comparison test, as indicated by the brackets (not statistically significant [ns], $p > 0.05$; *$p \leq 0.05$; **$p \leq 0.01$; ***$p \leq 0.001$).

while both interventions attenuate ASC speck formation in the BM niche, SLN124 exerts a broader anti-inflammatory effect that extends to extramedullary sites. Importantly, SLN124-mediated TMPRSS6 inhibition significantly reduced ASC speck formation in splenic CD45$^+$ cells, despite the presence of tissue iron loading, demonstrating attenuation of inflammasome activity even within iron-rich environments. These observations suggest that the effects of SLN124 on inflammasome activity are not solely attributable to iron reduction but may involve additional iron-independent immunoregulatory mechanisms.

10968652, 0, Downloaded from https://onlinelibrary.wiley.com/doi/10.1002/ajh.70391 by Alberto Martinez - NICE, National Institute for Health and Care Excellence , Wiley Online Library on [08/06/2026]. See the Terms and Conditions (https://onlinelibrary.wiley.com/terms-and-conditions) on Wiley Online Library for rules of use; OA articles are governed by the applicable Creative Commons License

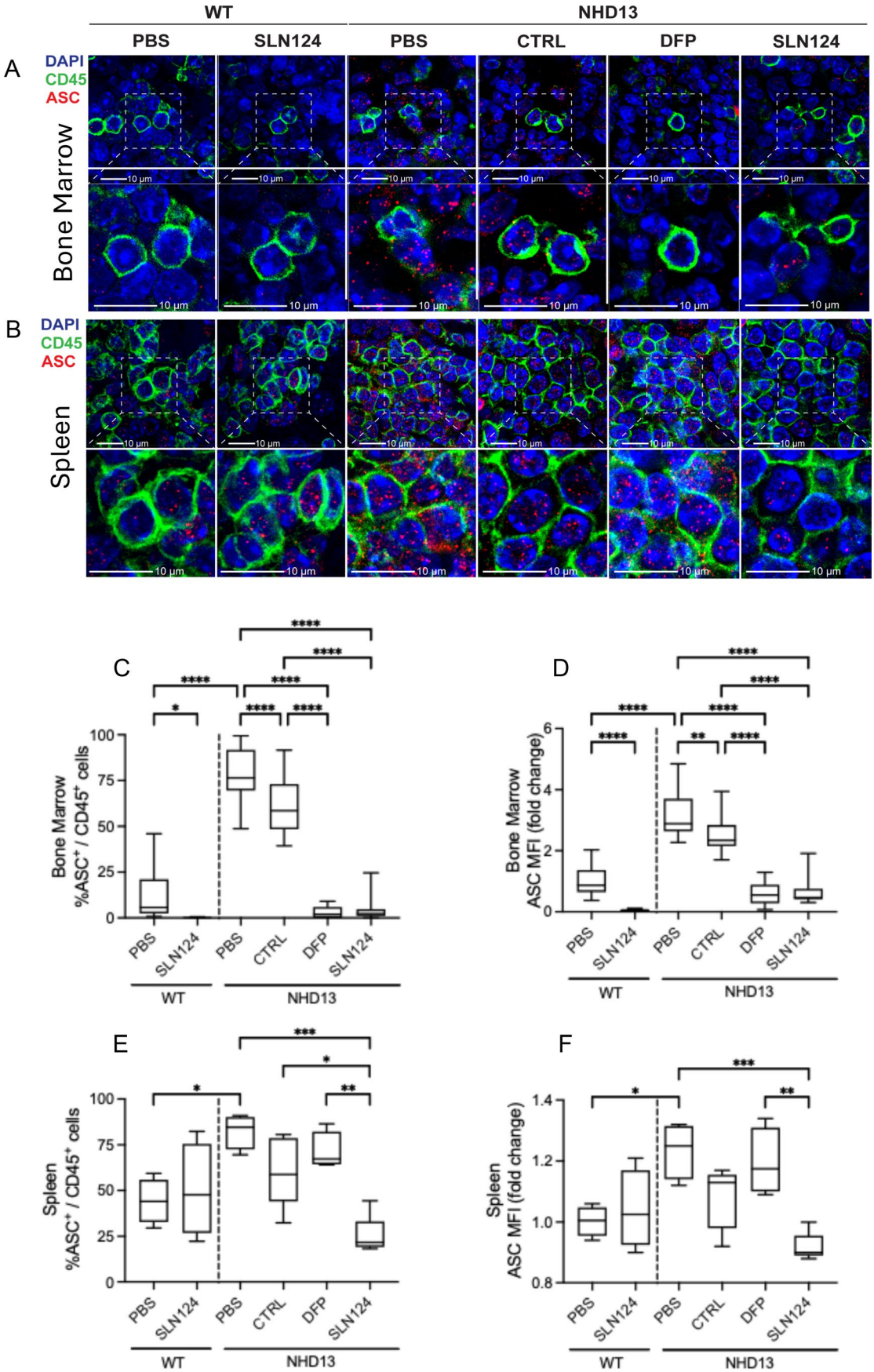


FIGURE 5 | Legend on next page.

10968652, 0, Downloaded from https://onlinelibrary.wiley.com/doi/10.1002/ajh.70391 by Alberto Martinez - NICE, National Institute for Health and Care Excellence , Wiley Online Library on [08/06/2026]. See the Terms and Conditions (https://onlinelibrary.wiley.com/terms-and-conditions) on Wiley Online Library for rules of use; OA articles are governed by the applicable Creative Commons License

FIGURE 5 | Iron restriction therapy reduces ASC-speck formation in MDS mice. Representative confocal image analysis of ASC expression in (A) BM and (B) spleen sections from treated and control groups. Mice received either SLN124 (3 mg/kg, subcutaneously on Days 0 and 28) or DFP administered in drinking water over a 60-day period. Control groups were given vehicle (PBS) or a nontargeting siRNA (CTRL). Expanded images are shown below. Immunofluorescence analysis of CD45 (green) and ASC (red) expression, merged with DAPI-stained nuclei (blue), demonstrates increased ASC specks in NHD13 mice compared to WT mice. Quantification of ASC expression in the BM (C, D) and spleen (E, F) was performed across WT and MDS treatment groups. Values represent the percentage of $CD45^+ASC^+$ cells and ASC mean fluorescence intensity (MFI) fold-change following treatment. BM and spleen immunofluorescence sections were analyzed using HALO software. Results are presented as box plots ($n = 4–5$ mice per group). Statistical significance was determined using one-way ANOVA followed by Bonferroni's post hoc test, as indicated by brackets (ns, $p > 0.05$; *$p \leq 0.05$; **$p \leq 0.01$; ***$p \leq 0.001$; ****$p \leq 0.001$).

3.8 | Iron Restriction Alters Subcellular ASC Speck Localization in $CD45^+$ Cells of MDS Mice

Translocation of ASC from the nucleus to the cytoplasm marks a critical shift from a primed, inactive state to an activated inflammasome complex [41–43]. Accordingly, the relative abundance of cytoplasmic versus nuclear/perinuclear ASC specks serves as a sensitive indicator of inflammasome activation intensity. To assess how iron restriction influences this process, we examined the subcellular distribution of ASC specks in $CD45^+$ hematopoietic cells from the bone marrow and spleen of MDS mice (Figures 6A,B and 4A,B). Quantitative image analysis using HALO software enabled distinction between nuclear/perinuclear (Figure 6C) and cytoplasmic (Figure 6D) ASC specks, corresponding to resting and activated inflammasome states, respectively [41–43]. In untreated and control siRNA-treated MDS mice, ASC specks were observed in both nuclear and cytoplasmic regions of $CD45^+$ cells from the BM and spleen, reflecting widespread inflammasome activation (Figure 6E,F). Treatment with either SLN124 or DFP significantly reduced the frequency of ASC^+ $CD45^+$ cells and decreased ASC speck abundance in both compartments in the BM (Figure 6E,F). Notably, SLN124 uniquely promoted nuclear retention of ASC specks, accompanied by reduced total ASC expression within $CD45^+$ cells in splenic tissue (Figure 6G,H). This pattern is indicative of a quiescent or inactive inflammasome state [41–43]. These findings indicate that SLN124-mediated TMPRSS6 inhibition not only suppresses ASC speck formation but also alters their subcellular localization in a manner consistent with reduced inflammasome activation. Collectively, our data support the conclusion that SLN124 attenuates inflammasome activity in $CD45^+$ cells through mechanisms extending beyond simple correction of iron overload. The observed anti-inflammatory effect likely reflects coordinated regulation of systemic, labile, and intracellular iron pools, integrated with modulation of immunometabolic reprogramming across $CD45^+$ leukocyte populations, including macrophages.

3.9 | Prolonged SLN124 Administration Promotes Erythroid Differentiation and Delays Disease Progression

Given the age-dependent progression of disease in MDS mice, where younger animals initially display preserved hematopoiesis but progressively develop cytopenias, dysplasia, and an increased risk of AML transformation with advancing age, targeting iron metabolism represents a rational strategy to delay disease onset and attenuate progression. To assess the impact of iron restriction on disease progression, SLN124 (3 mg/kg) was administered via monthly subcutaneous injections to MDS mice beginning at 180 days of age. Outcomes were compared with mice receiving the oral iron chelator DFP (1.25 mg/mL in drinking water) and with vehicle or control siRNA-treated MDS cohorts. Mice were monitored longitudinally by FBE between 6 and 12 months of age (Figure 7A–C).

At treatment initiation, MDS mice exhibited minimal signs of anemia, with Hb, Hct, MCV and RDW values comparable to WT and control groups (Figure 7A–C). By 9 months, hallmark features of anemia emerged, including reduced Hb and Hct and elevated MCV (Figure 7A–C). A significant increase in RDW was observed in NHD13 mice following SLN124 treatment. This change alone does not indicate altered disease progression, but rather, it likely reflects an effect on general iron restriction, as a similar increase was observed in SLN124-treated wild-type controls. By 12 months of age, SLN124-treated MDS mice showed clear evidence of delayed disease progression, characterized by significantly, higher Hb and Hct, and preserved MCV relative to both DFP-treated and control groups, consistent with attenuation of the progressive anemia typically observed in this model (Figure 7A–C).

We also quantified the relative proportions of myeloid populations in the peripheral blood of MDS mice. Consistent with the established biology of MDS, MDS mice exhibited a marked myeloid bias compared with wild-type controls, characterized by an increased proportion of circulating monocytes [21]. Notably, SLN124 treatment was associated with a partial attenuation of this myeloid skewing at 9-months of age, reflected by a reduction in the relative expansion of circulating monocytes (Figure S5). However, this effect was not sustained with continued SLN124 treatment, as monocyte and neutrophil proportions were comparable between treated and untreated MDS cohorts at 10-months of age.

To evaluate the long-term impact of iron restriction on disease progression, we assessed erythropoietic maturation, and survival in MDS mice following treatment with SLN124 or DFP. At experimental endpoint, flow cytometric analysis revealed a substantial accumulation of immature erythroid precursors, particularly basophilic and polychromatic erythroblasts, within the BM and spleen, accompanied by a marked reduction in terminal RBC maturation in MDS mice (Figures 7D,E and S6A,B). SLN124-treated MDS mice exhibited a markedly enhanced erythroid maturation profile, characterized by a pronounced reduction in immature erythroblasts and a corresponding increase in mature erythroid

10968652, 0, Downloaded from https://onlinelibrary.wiley.com/doi/10.1002/ajh.70391 by Alberto Martinez - NICE, National Institute for Health and Care Excellence , Wiley Online Library on [08/06/2026]. See the Terms and Conditions (https://onlinelibrary.wiley.com/terms-and-conditions) on Wiley Online Library for rules of use; OA articles are governed by the applicable Creative Commons License

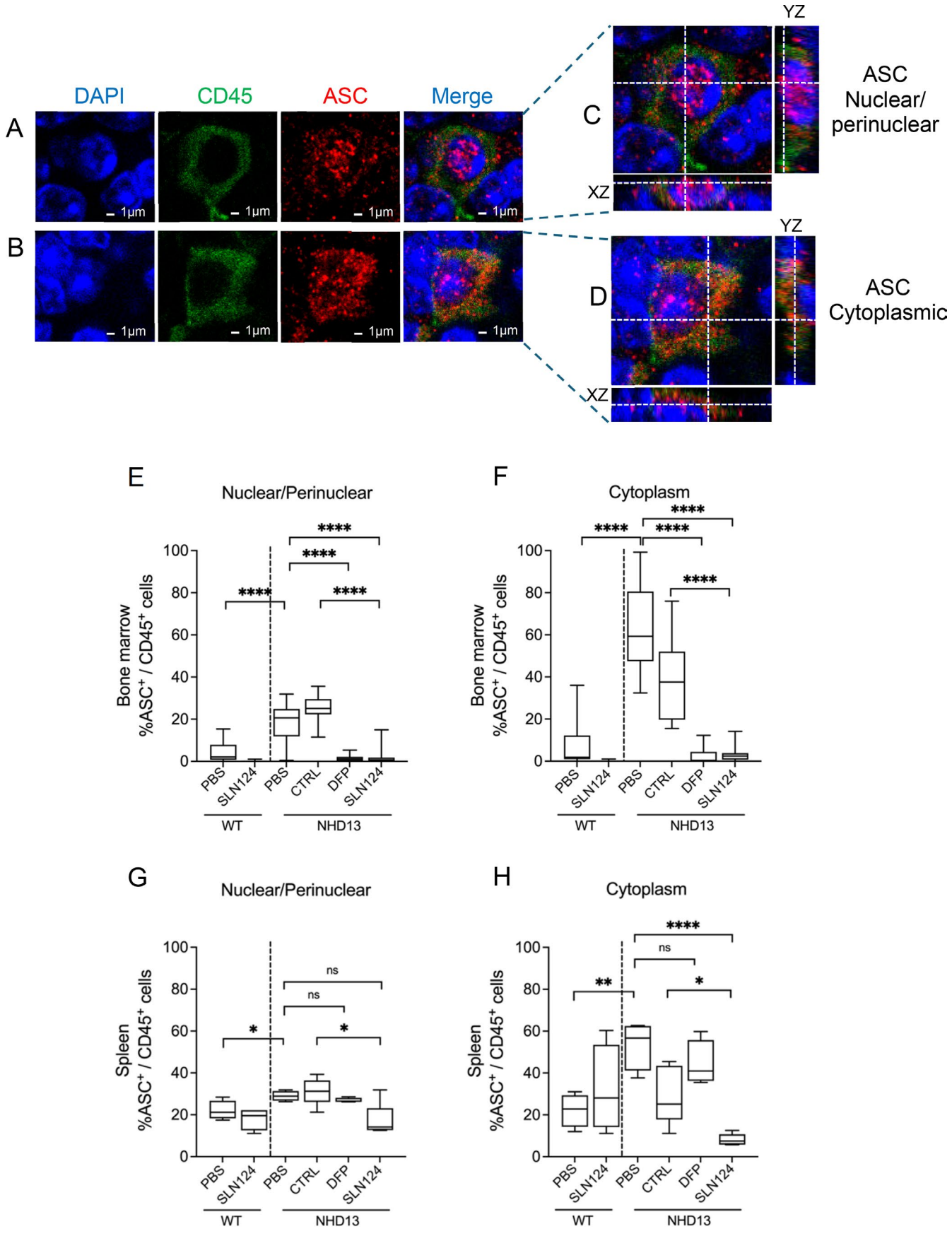


FIGURE 6 | Legend on next page.

10968652, 0, Downloaded from https://onlinelibrary.wiley.com/doi/10.1002/ajh.70391 by Alberto Martinez - NICE, National Institute for Health and Care Excellence , Wiley Online Library on [08/06/2026]. See the Terms and Conditions (https://onlinelibrary.wiley.com/terms-and-conditions) on Wiley Online Library for rules of use; OA articles are governed by the applicable Creative Commons License

FIGURE 6 | Iron restriction reduces cytoplasmic ASC speck distribution in CD45$^+$ cells from MDS mice. Representative confocal immunofluorescence analysis showing intracellular ASC speck localization in CD45$^+$ cells from treated and control groups. NHD13 mice received SLN124 (3 mg/kg, subcutaneously on Days 0 and 28) over 60 days. Control groups were given vehicle (PBS) or a nontargeting siRNA (CTRL). Cells positive for nuclear/perinuclear or cytoplasmic ASC specks were quantified in BM and spleen sections using HALO software. (A) Top panels show ASC speck nuclear/perinuclear localization, while (B) bottom panels show cytoplasmic ASC speck distribution in CD45$^+$ cells from MDS mice. Orthogonal projections from z-stack confocal images analysis illustrate (C) nuclear/perinuclear and (D) cytoplasmic ASC speck distribution in CD45$^+$ cells. (E) Quantification of nuclear/perinuclear and (F) cytoplasmic ASC speck distribution in bone marrow CD45$^+$ cells from WT and NHD13 mice. (G) Quantification of nuclear/perinuclear and (H) cytoplasmic ASC speck distribution in splenic CD45$^+$ cells from WT and NHD13 mice. Immunofluorescence staining was performed for CD45 (green) and ASC (red), with nuclei counterstained using DAPI (blue). Results are presented as box-and-whisker plots ($n = 4–5$ mice per group). Statistical comparisons of intergroup differences in nuclear/perinuclear or cytoplasmic ASC speck localization were performed using one-way ANOVA followed by Bonferroni's post hoc test (ns, not significant, $p > 0.05$; *$p \leq 0.05$; **$p \leq 0.01$; ***$p \leq 0.001$; ****$p \leq 0.0001$).

populations in the spleen, but not in the BM, compared with vehicle- and control siRNA-treated groups (Figures 7D,E and S6A,B).

Survival analysis demonstrated that all vehicle- and DFP-treated MDS mice succumbed by Day 420, whereas SLN124 conferred a survival advantage, with 5 of 16 mice surviving to Day 450 (Figure 7G,H). In parallel, SLN124-treated mice exhibited a reduced spleen-to-body weight ratio at Day 450, consistent with attenuation of disease burden (Figure 7F). The associated extension in survival supports a disease-modifying effect of TMPRSS6 inhibition, potentially mediated through suppression of inflammatory activity, altered tissue iron distribution, and delayed progression of hematological decline. Collectively, these findings support therapeutic targeting of the TMPRSS6–hepcidin axis as a viable early intervention strategy to delay disease progression and reduce iron-mediated inflammatory burden in MDS.

4 | Discussion

In our studies, we systematically investigated the therapeutic potential of iron restriction through selective modulation of the TMPRSS6-hepcidin regulatory axis and its impact on hematopoietic function and disease trajectory in MDS. Using the well-established MDS murine model, we demonstrated that treatment with a GalNAc-conjugated small interfering RNA targeting *Tmprss6* induced a sustained upregulation of endogenous hepcidin, effectively reducing systemic iron availability, and attenuated iron-driven inflammation. Notably, this intervention significantly prolonged survival, underscoring the disease-modifying potential of TMPRSS6 inhibition. Mechanistically, SLN124 treatment reduced inflammasome activation and ameliorated hematopoietic dysfunction, supporting a functional link between iron dysregulation, innate immune activation, and ineffective hematopoiesis. These findings are consistent with the concept that excess bioavailable iron amplifies inflammatory stress within the hematopoietic microenvironment, thereby exacerbating marrow dysfunction and disease severity [20, 21]. Collectively, these findings provide mechanistic support for targeting the TMPRSS6-hepcidin axis to mitigate iron-mediated toxicity, reprogram the pro-inflammatory hematopoietic microenvironment and thereby contribute to disease modification and delayed progression in MDS.

While the NHD13 transgenic mouse remains one of the most extensively characterized murine models of MDS, recapitulating key clinical, morphological, and hematopoietic features of the human disease, it has limitations in its genetic relevance. Specifically, the model is driven by the NUP98–HOXD13 fusion, a rare cytogenetic abnormality in human MDS patients, limiting its representation of the broader mutational landscape observed in clinical cohorts [44]. Despite this, the pathogenic mechanisms identified in the MDS model are supported by independent studies in genetically diverse systems. In particular, Basiorka et al. demonstrated that activation of the inflammasome-pyroptosis axis is a common, unifying feature of MDS, occurring independently of the functional class of underlying somatic mutations [9, 13]. Using both murine and transduced cell line models, they showed that HSPCs bearing mutations in RNA splicing factors (*U2AF1, SF3B1, SRSF2*) and epigenetic regulators (*ASXL1, TET2*) uniformly exhibited heightened pyroptotic activity [9, 13, 14]. Importantly, these pyroptotic phenotypes were significantly suppressed by inhibition of the NLRP3 inflammasome or blockade of NADPH oxidase–dependent ROS production, identifying oxidative stress as a common upstream trigger. This suggests that, despite their functional diversity, MDS-associated mutations converge on a shared inflammasome-pyroptosis pathway [9, 13, 14].

ASC is a central adaptor protein in inflammasome complexes that forms large aggregates, approximately 1–2 μm in diameter, termed as ASC specks. ASC acts as a molecular scaffold for the assembly of inflammasome components, including NOD-like receptors (NLRs). This assembly leads to the activation of caspase-1, resulting in IL-1β/IL-18 maturation and the induction of pyroptotic cell death [45]. ASC is also an important adaptor for a range of other NLRs, including NLRP1, AIM2, Pyrin, NLRC4 and newly discovered NLRP10 [46]. Therefore, ASC specks serve as direct and quantifiable indicator of inflammasome activation, and subsequent pyroptotic cell death [45]. Clinical studies have demonstrated that plasma ASC speck levels are significantly elevated in patients with MDS compared to age-matched healthy controls [13, 14]. Intriguingly, ASC speck burden was highest among patients with lower-risk MDS (LR-MDS), suggesting that pyroptosis is particularly active in early disease stages, potentially contributing to cytopenias and ineffective hematopoiesis [13]. Moreover, the proportion of ASC specks in plasma correlated directly with the number of somatic mutations, highlighting

10968652, 0, Downloaded from https://onlinelibrary.wiley.com/doi/10.1002/ajh.70391 by Alberto Martinez - NICE, National Institute for Health and Care Excellence , Wiley Online Library on [08/06/2026]. See the Terms and Conditions (https://onlinelibrary.wiley.com/terms-and-conditions) on Wiley Online Library for rules of use; OA articles are governed by the applicable Creative Commons License

a quantitative relationship between clonal complexity and inflammasome activity [13]. In agreement with observations in MDS patients, our study shows that ASC speck formation in CD45$^+$ hematopoietic cells is elevated in MDS mice and positively correlated with iron deposits in the BM and spleen in the early stages of disease.

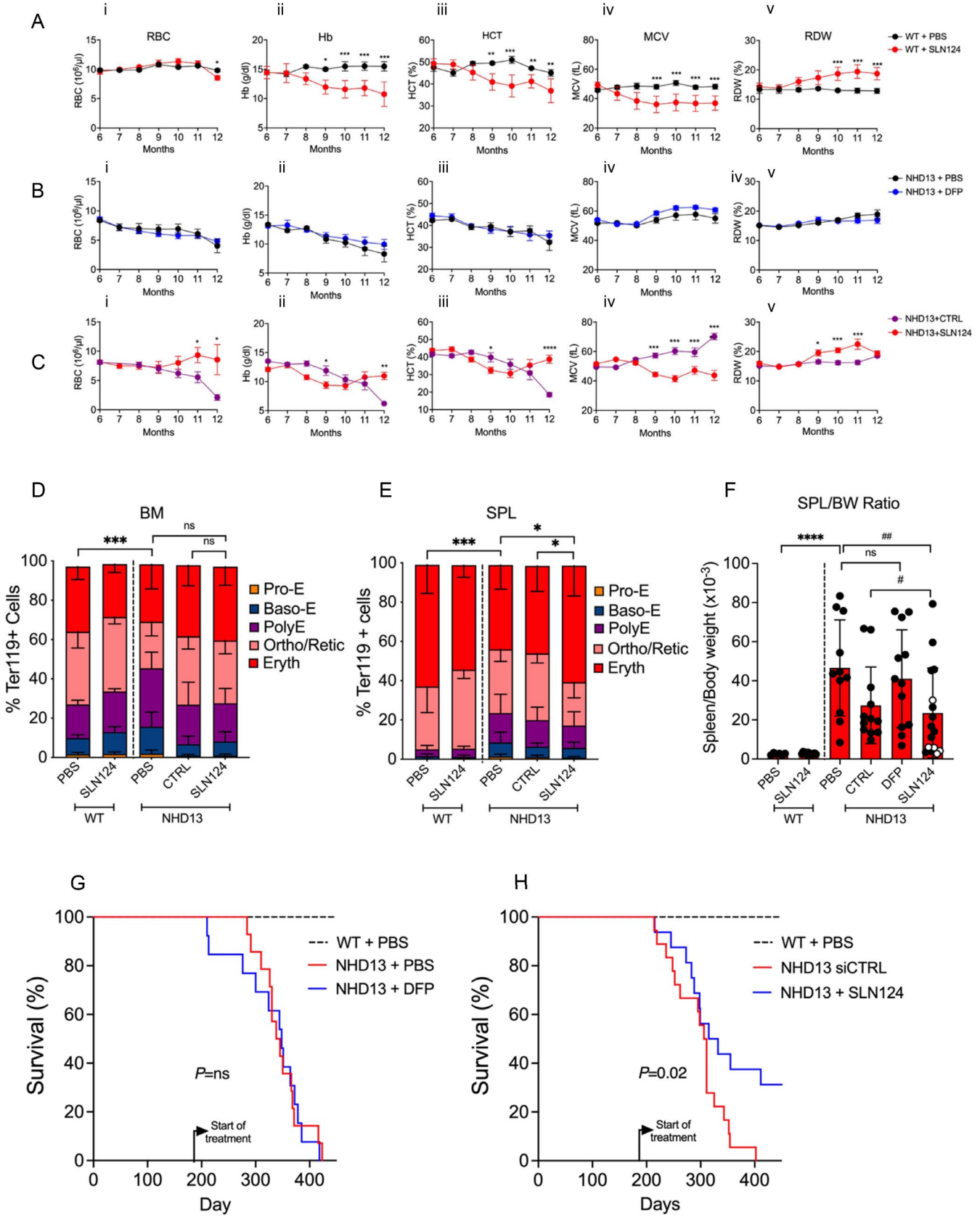


FIGURE 7 | Legend on next page.

10968652, 0, Downloaded from https://onlinelibrary.wiley.com/doi/10.1002/ajh.70391 by Alberto Martinez - NICE, National Institute for Health and Care Excellence , Wiley Online Library on [08/06/2026]. See the Terms and Conditions (https://onlinelibrary.wiley.com/terms-and-conditions) on Wiley Online Library for rules of use; OA articles are governed by the applicable Creative Commons License

FIGURE 7 | SLN124 reduces ineffective erythropoiesis and provides a survival advantage in MDS mice. For long-term studies, WT and MDS mice received monthly subcutaneous injections of SLN124 (3 mg/kg) starting at 6 months of age and continuing until study endpoint. A separate cohort of MDS mice received deferiprone (DFP; 1.25 mg/mL) in drinking water during the same period. Control groups were treated with vehicle (PBS) or a nontargeting siRNA (CTRL). Peripheral blood was analyzed monthly by full blood examination (FBE), and BM and spleen samples were collected at endpoint for analysis. (A–C) Analysis of red blood cell parameters (i) red blood cell counts, (ii) hemoglobin (Hb), (iii) hematocrit (HCT), (iv) mean cellular volume (MCV), and (v) red cell distribution width (RDW). Proportions of erythroid subpopulations in the (D) BM, (E) spleen and (F) spleen/body weight ratio of WT and NHD13 mice at study endpoint. Open circles denote SLN124-treated MDS mice that survived to 450 days. Control groups were treated with either vehicle (PBS) or non-targeting siRNA (CTRL). Flow cytometric analysis of erythroid cells at different stages of maturation was performed using Ter119 and CD44-labeled antibodies. Forward scatter (FSC) was used to distinguish five distinct stages of erythroid differentiation: (i) proerythroblasts, (ii) basophilic, (iii) polychromatic, (iv) orthochromatic reticulocytes, and (v) mature red blood cells (RBCs). Data are presented as stacked bar graphs with mean ± SEM. Statistical analysis was determined by one-way ANOVA followed by Bonferroni's post hoc test (ns, $p > 0.05$; *$p \leq 0.05$; **$p \leq 0.01$; ***$p \leq 0.001$; ****$p \leq 0.0001$) and ($^{\#}p \leq 0.05$; $^{\#\#}p \leq 0.01$) denotes comparison with mice surviving to 450 days (open circles). (G) Kaplan–Meier survival curve showing the percentage of survival in NHD13 mice receiving either vehicle (PBS) ($n = 13$) or DFP (1.25 mg/mL) in the drinking water ($n = 15$). (H) Kaplan–Meier survival curves of NHD13 mice treated with either control siRNA (siCTRL) ($n = 17$) or SLN124 (3 mg/kg) ($n = 16$). siCTRL and SLN124 were administered subcutaneously every month from 6 to 14 months of age. Mice were observed for up to 450 days. Statistical analysis comparing the survival curves was performed using the log-rank (Mantel–Cox) test.

Previous studies have reported that ASC translocation from the nucleus/perinuclear space to the cytosol is required for inflammasome assembly [41, 47–49]. Our findings revealed two distinct patterns of ASC speck subcellular localization, either confined to the nuclear/perinuclear space, or dispersed throughout the cytosol, with the latter consistent with active inflammasome assembly and activation [41, 47–50]. This spatial regulation of ASC is tightly governed by posttranslational modifications (PTMs), including phosphorylation, ubiquitination, and SUMOylation, which collectively modulate ASC's stability, distribution, and ability to nucleate inflammasome complexes [43, 51–53]. These PTM-mediated mechanisms act as critical checkpoints to restrict inflammasome activation under homeostatic conditions [41, 47]. Experimental inhibition of ASC nuclear-cytosolic translocation has been shown to prevent ASC speck formation and inhibit inflammasome activity, highlighting the requirement for cytosolic localization for initiating inflammatory responses [49, 54].

This regulatory control is particularly vital, as HSPCs are highly susceptible to inflammation-induced pyroptotic cell death [41, 47]. In MDS, this protective barrier may be compromised by chronic cellular stressors, including somatic mutations, excess labile iron, and oxidative damage. Therefore, loss of nuclear/perinuclear retention of ASC may facilitate aberrant cytosolic accumulation, inappropriate inflammasome activation, and downstream effects such as pyroptotic cell death, ineffective hematopoiesis, and clonal expansion [55, 56]. Our study in MDS mice demonstrates that early therapeutic iron restriction attenuated ASC speck formation and significantly reduced cytosolic ASC localization in BM CD45^{+} hematopoietic cells. In contrast, these effects in the spleen were observed only with SLN124 treatment, which led to a significant reduction in overall ASC speck formation accompanied by decreased cytosolic ASC localization in splenic CD45^{+} cells.

Most notably, SLN124 treatment produced the greatest reduction in ASC speck formation and significantly decreased cytosolic localization of ASC, particularly in the spleen, compared to DFP. In parallel, SLN124 conferred a significant survival benefit in MDS mice, reinforcing the role of iron-driven inflammatory mechanisms in early disease progression, well before the onset of overt cytopenias. Targeting iron dysregulation early in the disease course may not only delay the onset or progression of anemia but also attenuate the inflammatory and pyroptotic cascades that underlie disease evolution. Beyond its established role in systemic iron regulation, TMPRSS6 inhibition can also exert anti-inflammatory effects. In preclinical models, both genetic ablation and suppression of TMPRSS6 expression studies result in significantly reduced expression of pro-inflammatory cytokines, including IL-6 and TNF-α [27, 57, 58]. These findings suggest that hepcidin induction following reduced TMPRSS6 expression restricts iron availability to myeloid cells, thereby dampening their metabolic inflammatory activity. Importantly, this mechanism highlights that therapeutic targeting of the TMPRSS6-hepcidin axis may not only restrain iron overload but also suppress aberrant myeloid cell activation, offering a potentially disease-modifying therapeutic strategy.

Recent advances have elucidated the central role of innate immune and pro-inflammatory signaling pathways in driving key pathogenic features of MDS [59, 60]. These insights have catalyzed the development of novel therapeutic strategies aimed at suppressing inflammation-mediated BM dysfunction and slow disease progression. One promising approach involves targeting IL-1β signaling. For example, canakinumab, a monoclonal antibody that neutralizes IL-1β, is currently being repurposed for clinical evaluation in MDS [61]. In addition, shared intracellular mediators of proinflammatory signaling, such as interleukin-1 receptor-associated kinases (IRAK1/4), have emerged as attractive therapeutic targets, with IRAK4 inhibitors under clinical investigation in MDS, with the aim of disrupting downstream NF-κB signaling and suppressing the expansion of MDS clones [62, 63]. Moreover, small molecule inhibitors of inflammasome-mediated pyroptosis such as MCC950 have demonstrated the ability to block NLRP3 inflammasome activation, reduce IL-1β release, and preserve HSPC integrity in MDS models [9, 63]. Collectively, these emerging therapies underscore the rationale for targeting inflammation in MDS, moving beyond traditional cytotoxic regimens toward targeted, anti-inflammatory approaches.

Myeloid skewing is also a recognized feature of MDS and reflects inflammatory remodeling of the hematopoietic hierarchy, with

10968652, 0, Downloaded from https://onlinelibrary.wiley.com/doi/10.1002/ajh.70391 by Alberto Martinez - NICE, National Institute for Health and Care Excellence , Wiley Online Library on [08/06/2026]. See the Terms and Conditions (https://onlinelibrary.wiley.com/terms-and-conditions) on Wiley Online Library for rules of use; OA articles are governed by the applicable Creative Commons License

preferential expansion of myeloid progenitors at the expense of effective erythropoiesis [21]. In our cohort, although iron restriction strategies modulated iron homeostasis and attenuated inflammasome activation, their impact on myeloid skewing was limited. This observation suggests that while iron-driven inflammatory signaling contributes to niche dysfunction, myeloid bias in MDS is likely sustained by additional mutation-associated and cytokine-mediated mechanisms that are not fully reversible through iron modulation alone. These findings underscore the multifactorial nature of lineage imbalance in MDS and highlight the need for combinatorial therapeutic approaches targeting both iron-dependent and iron-independent drivers of clonal myeloid expansion.

By leveraging a preclinical model of pathophysiological iron overload with pharmacologically induced iron restriction these studies provide mechanistic insights into the contribution of iron dysregulation to MDS pathogenesis and support a proof-of-concept for early therapeutic intervention. Our findings demonstrate that iron restriction, particularly with SLN124, was associated with attenuation of inflammasome activation, evidenced by reduced ASC speck formation and cytosolic redistribution, and with prolonged survival supporting a functional link between iron homeostasis and inflammatory signaling. Defining the timing, intensity, and duration of iron restriction will be important to establish an optimal therapeutic window for clinical translation.

Several important limitations warrant consideration. The use of standard normal chow, representing relatively high iron exposure, likely contributed to the absence of overt anemia at 6 months in NHD13 mice and may confound assessment of therapeutic efficacy [20, 21]. These findings underscore dietary iron as an important experimental variable when interpreting iron-targeted interventions. In addition, cell type-specific resolution of iron distribution was not defined. Although DFP and SLN124 alter tissue iron, the compartments that become iron-deficient or retain iron remain unclear, limiting mechanistic distinction between intracellular chelation and systemic iron restriction. Consistent with this, while SLN124 reduces plasma and BM iron, the fate of this iron is not established. As iron is not actively excreted and changes in absorption are not addressed, it is unclear whether iron is redistributed to other compartments. Ineffective erythropoiesis was not extensively quantified, limiting interpretation of the reported improvements and necessitating validation using erythroid-specific and apoptotic markers, including erythroferrone expression. In addition, there is no direct evidence for BM iron restriction with SLN124, and this will require confirmation with direct measures of iron availability and utilization.

In conclusion, our results highlight the biological and therapeutic significance of iron modulation in MDS and strengthen the rationale for early, preemptive iron-lowering interventions. Such approaches may be particularly beneficial in LR-MDS patients with symptomatic anemia, in whom disease burden is often underestimated and treatment initiation deferred [3]. In the setting of an aging population with increasing MDS prevalence and limited disease-modifying options, therapeutic modulation of TMPRSS6, either as monotherapy or in combination with agents targeting complementary pathogenic pathways, has the potential to reshape disease trajectory, delay progression to AML, and ultimately improve survival and patient-reported outcomes.

Author Contributions

Jim Vadolas, Shahla Vilcassim, Alberto Martinez, Ute Schaeper, and George Grigoriadis conceived and designed the research project. Experimental work was carried out by Jim Vadolas, Nuttanan Pholngam, Rattanawan Thubthed, Tiwaporn Nualkaew, Peter J. Crouch, Kai Kysenius, and Mona Eisermann. Sibylle Dames designed the siRNA sequences and performed the statistical analyses. The manuscript was written by Jim Vadolas, George Grigoriadis, and Shahla Vilcassim. All authors reviewed and approved the final manuscript. Kai Kysenius is affiliated with Eli Lilly, Finland.

Acknowledgments

Jim Vadolas acknowledges funding from Silence Therapeutics Plc, London, UK and mRNA Victoria Research Acceleration Fund (mVRAF), Australia. Nuttanan Pholngam was supported by the Royal Golden Jubilee PhD Research Scholarship, the National Research Council of Thailand (NRCT), and the Thailand Research Fund (TRF) (Grant no. PHD/0054/2561, Code no. 4.U.MU/61/C.1.O.XX). Monash Pathology for granting access to their facilities and equipment. The DFP was kindly provided by ApoPharma Inc., Toronto, ON, Canada. Open access publishing facilitated by Monash University, as part of the Wiley - Monash University agreement via the Council of Australasian University Librarians.

Funding

Jim Vadolas acknowledges funding from Silence Therapeutics Plc, London, UK and mRNA Victoria Research Acceleration Fund (mVRAF), Australia. Nuttanan Pholngam was supported by the Royal Golden Jubilee PhD Research Scholarship, the National Research Council of Thailand (NRCT) and the Thailand Research Fund (TRF) (Grant no. PHD/0054/2561, Code no. 4.U.MU/61/C.1.O.XX).

Ethics Statement

All animal experiments were conducted in accordance with institutional guidelines and approved by the Monash Health Animal Ethics Committee. Studies were performed under ethics approval number MMCA/2019/26, granted to the Monash Health Research Precinct, Monash Medical Centre.

Conflicts of Interest

Co-authors Ute Schaeper, Sibylle Dames, Mona Eisermann, and Alberto Martinez are employees and stock option holders of Silence Therapeutics GmbH or Plc.

Data Availability Statement

The data that supports the findings of this study are available in the S1 of this article.

References

1. P. Fenaux and L. Adès, "How We Treat Lower-Risk Myelodysplastic Syndromes," *Blood* 121, no. 21 (2013): 4280–4286.

2. N. Gattermann, "Iron Overload in Myelodysplastic Syndromes (MDS)," *International Journal of Hematology* 107, no. 1 (2018): 55–63.

3. U. Germing, E. N. Oliva, D. Hiwase, and A. Almeida, "Treatment of Anemia in Transfusion-Dependent and Non-Transfusion-Dependent Lower-Risk MDS: Current and Emerging Strategies," *HemaSphere* 3, no. 6 (2019): e314.

10968652, 0, Downloaded from https://onlinelibrary.wiley.com/doi/10.1002/ajh.70391 by Alberto Martinez - NICE, National Institute for Health and Care Excellence , Wiley Online Library on [08/06/2026]. See the Terms and Conditions (https://onlinelibrary.wiley.com/terms-and-conditions) on Wiley Online Library for rules of use; OA articles are governed by the applicable Creative Commons License

4. S. Weber, A. Parmon, N. Kurrle, F. Schnutgen, and H. Serve, "The Clinical Significance of Iron Overload and Iron Metabolism in Myelodysplastic Syndrome and Acute Myeloid Leukemia," *Frontiers in Immunology* 11 (2020): 627662.

5. C. Camaschella, A. Nai, and L. Silvestri, "Iron Metabolism and Iron Disorders Revisited in the Hepcidin Era," *Haematologica* 105, no. 2 (2020): 260–272.

6. S. Kikuchi, M. Kobune, S. Iyama, et al., "Improvement of Iron-Mediated Oxidative DNA Damage in Patients With Transfusion-Dependent Myelodysplastic Syndrome by Treatment With Deferasirox," *Free Radical Biology and Medicine* 53, no. 4 (2012): 643–648.

7. I. Ganan-Gomez, Y. Wei, D. T. Starczynowski, et al., "Deregulation of Innate Immune and Inflammatory Signaling in Myelodysplastic Syndromes," *Leukemia* 29, no. 7 (2015): 1458–1469.

8. T. Jiménez-Solas, F. López-Cadenas, I. Aires-Mejía, et al., "Deferasirox Reduces Oxidative DNA Damage in Bone Marrow Cells From Myelodysplastic Patients and Improves Their Differentiation Capacity," *British Journal of Haematology* 187, no. 1 (2019): 93–104.

9. A. A. Basiorka, K. L. McGraw, E. A. Eksioglu, et al., "The NLRP3 Inflammasome Functions as a Driver of the Myelodysplastic Syndrome Phenotype," *Blood* 128, no. 25 (2016): 2960–2975.

10. M. Schneider, C. Rolfs, M. Trumpp, et al., "Activation of Distinct Inflammatory Pathways in Subgroups of LR-MDS," *Leukemia* 37, no. 8 (2023): 1709–1718.

11. M. T. Villaume and M. R. Savona, "Pathogenesis and Inflammaging in Myelodysplastic Syndrome," *Haematologica* 110, no. 2 (2025): 283–299.

12. R. C. Coll and K. Schroder, "Inflammasome Components as New Therapeutic Targets in Inflammatory Disease," *Nature Reviews Immunology* 25, no. 1 (2025): 22–41.

13. A. A. Basiorka, K. L. McGraw, F. Abbas-Aghababazadeh, et al., "Assessment of ASC Specks as a Putative Biomarker of Pyroptosis in Myelodysplastic Syndromes: An Observational Cohort Study," *Lancet Haematology* 5, no. 9 (2018): e393–e402.

14. D. A. Sallman and A. List, "The Central Role of Inflammatory Signaling in the Pathogenesis of Myelodysplastic Syndromes," *Blood* 133, no. 10 (2019): 1039–1048.

15. J. Topping, A. Taylor, F. Nadat, et al., "Inflammatory Profile of Lower Risk Myelodysplastic Syndromes," *British Journal of Haematology* 205, no. 3 (2024): 1044–1054.

16. A. Baroja-Mazo, F. Martín-Sánchez, A. I. Gomez, et al., "The NLRP3 Inflammasome Is Released as a Particulate Danger Signal That Amplifies the Inflammatory Response," *Nature Immunology* 15, no. 8 (2014): 738–748.

17. B. S. Franklin, L. Bossaller, D. De Nardo, et al., "The Adaptor ASC Has Extracellular and 'prionoid' Activities That Propagate Inflammation," *Nature Immunology* 15, no. 8 (2014): 727–737.

18. A. Harijith, D. L. Ebenezer, and V. Natarajan, "Reactive Oxygen Species at the Crossroads of Inflammasome and Inflammation," *Frontiers in Physiology* 5 (2014): 352.

19. J. Xin, H. Xiaoyuan, C. Xiaoli, et al., "Iron Overload Impairs Normal Hematopoietic Stem and Progenitor Cells Through Reactive Oxygen Species and Shortens Survival in Myelodysplastic Syndrome Mice," *Haematologica* 103, no. 10 (2018): 1627–1634.

20. W. An, M. Feola, M. Levy, et al., "Iron Chelation Improves Ineffective Erythropoiesis and Iron Overload in Myelodysplastic Syndrome Mice," *eLife* 12 (2023): e83103.

21. A. Antypiuk, S. Z. Vance, R. Sharma, et al., "Genetic Iron Overload Aggravates, and Pharmacological Iron Restriction Improves, MDS Pathophysiology in a Preclinical Study," *Blood* 145, no. 2 (2025): 155–169.

22. A. Banerjee, N. A. Mifsud, R. Bird, et al., "The Oral Iron Chelator Deferasirox Inhibits NF-kappaB Mediated Gene Expression Without Impacting on Proximal Activation: Implications for Myelodysplasia and Aplastic Anaemia," *British Journal of Haematology* 168, no. 4 (2015): 576–582.

23. E. N. Oliva, F. Ronco, A. Marino, C. Alati, G. Praticò, and F. Nobile, "Iron Chelation Therapy Associated With Improvement of Hematopoiesis in Transfusion-Dependent Patients," *Transfusion* 50, no. 7 (2010): 1568–1570.

24. R. M. Lyons, B. J. Marek, C. Paley, et al., "Comparison of 24-Month Outcomes in Chelated and Non-Chelated Lower-Risk Patients With Myelodysplastic Syndromes in a Prospective Registry," *Leukemia Research* 38, no. 2 (2014): 149–154.

25. N. Shenoy, N. Vallumsetla, E. Rachmilewitz, A. Verma, and Y. Ginzburg, "Impact of Iron Overload and Potential Benefit From Iron Chelation in Low-Risk Myelodysplastic Syndrome," *Blood* 124, no. 6 (2014): 873–881.

26. M. Pettinato, V. Furiosi, R. Carleo, et al., "Targeting the Liver Serine Protease TMPRSS6 Ameliorates Steatosis and Attenuates Fibrosis in Experimental MASLD," *Liver International* 45, no. 7 (2025): e70163.

27. M. Riba, M. Rausa, M. Sorosina, et al., "A Strong Anti-Inflammatory Signature Revealed by Liver Transcription Profiling of Tmprss6−/− Mice," *PLoS One* 8, no. 7 (2013): e69694.

28. S. Altamura, U. Schaeper, S. Dames, et al., "SLN124, a GalNAc-siRNA Conjugate Targeting TMPRSS6, Efficiently Prevents Iron Overload in Hereditary Haemochromatosis Type 1," *Hema* 3, no. 6 (2019): e301.

29. J. B. Porter, A. Scrimgeour, A. Martinez, et al., "SLN124, a GalNAc Conjugated 19-Mer siRNA Targeting tmprss6, Reduces Plasma Iron and Increases Hepcidin Levels of Healthy Volunteers," *American Journal of Hematology* 98, no. 9 (2023): 1425–1435.

30. J. Vadolas, G. Z. Ng, K. Kysenius, et al., "SLN124, a GalNac-siRNA Targeting Transmembrane Serine Protease 6, in Combination With Deferiprone Therapy Reduces Ineffective Erythropoiesis and Hepatic Iron-Overload in a Mouse Model of Beta-Thalassaemia," *British Journal of Haematology* 194, no. 1 (2021): 200–210.

31. Y.-W. Lin, C. Slape, Z. Zhang, and P. D. Aplan, "NUP98-HOXD13 Transgenic Mice Develop a Highly Penetrant, Severe Myelodysplastic Syndrome That Progresses to Acute Leukemia," *Blood* 106, no. 1 (2005): 287–295.

32. W. Yang, C. Xiao, J. Zheng, J. Song, and X. G. Li, "Copper Homeostasis and Cuproptosis Represent Emerging Targets for Therapeutic Intervention in Inflammatory Diseases," *Pharmacological Research* 221 (2025): 107988.

33. K. Jomova, S. Y. Alomar, R. Valko, E. Nepovimova, K. Kuca, and M. Valko, "The Role of Redox-Active Iron, Copper, Manganese, and Redox-Inactive Zinc in Toxicity, Oxidative Stress, and Human Diseases," *EXCLI Journal* 24 (2025): 880–954.

34. M. Sapkota and D. L. Knoell, "Essential Role of Zinc and Zinc Transporters in Myeloid Cell Function and Host Defense Against Infection," *Journal of Immunology Research* 2018 (2018): 4315140.

35. W. Kuzmicka, A. Manda-Handzlik, A. Cieloch, et al., "Zinc Supplementation Modulates NETs Release and Neutrophils' Degranulation," *Nutrients* 13, no. 1 (2021): 51.

36. S. Ni, Y. Yuan, Y. Kuang, and X. Li, "Iron Metabolism and Immune Regulation," *Frontiers in Immunology* 13 (2022): 816282.

37. E. A. Osterholm and M. K. Georgieff, "Chronic Inflammation and Iron Metabolism," *Journal of Pediatrics* 166, no. 6 (2015): 1351–1357. e1351.

10968652, 0, Downloaded from https://onlinelibrary.wiley.com/doi/10.1002/ajh.70391 by Alberto Martinez - NICE, National Institute for Health and Care Excellence , Wiley Online Library on [08/06/2026]. See the Terms and Conditions (https://onlinelibrary.wiley.com/terms-and-conditions) on Wiley Online Library for rules of use; OA articles are governed by the applicable Creative Commons License

38. M. Byrne, R. L. Bennett, X. Cheng, and W. S. May, "Progressive Genomic Instability in the Nup98-HoxD13 Model of MDS Correlates With Loss of the PIG-A Gene Product," *Neoplasia* 16, no. 8 (2014): 627–633.

39. Q. Ye, J. E. Park, K. Gugnani, S. Betharia, A. Pino-Figueroa, and J. Kim, "Influence of Iron Metabolism on Manganese Transport and Toxicity," *Metallomics* 9, no. 8 (2017): 1028–1046.

40. Q. Liu, S. Barker, and M. D. Knutson, "Iron and Manganese Transport in Mammalian Systems," *Biochimica et Biophysica Acta, Molecular Cell Research* 1868, no. 1 (2021): 118890.

41. N. B. Bryan, A. Dorfleutner, Y. Rojanasakul, and C. Stehlik, "Activation of Inflammasomes Requires Intracellular Redistribution of the Apoptotic Speck-Like Protein Containing a Caspase Recruitment Domain," *Journal of Immunology (Baltimore, MD: 1950)* 182, no. 5 (2009): 3173–3182.

42. D. P. Sester, S. J. Thygesen, V. Sagulenko, et al., "A Novel Flow Cytometric Method to Assess Inflammasome Formation," *Journal of Immunology* 194, no. 1 (2015): 455–462.

43. D. Dong, Y. Du, X. Fei, et al., "Inflammasome Activity Is Controlled by ZBTB16-Dependent SUMOylation of ASC," *Nature Communications* 14, no. 1 (2023): 8465.

44. S. Ogawa, "Genetics of MDS," *Blood* 133, no. 10 (2019): 1049–1059.

45. A. Nagar, R. Bharadwaj, M. O. F. Shaikh, and A. Roy, "What Are NLRP3-ASC Specks? An Experimental Progress of 22 Years of Inflammasome Research," *Frontiers in Immunology* 14 (2023): 1188864.

46. T. Próchnicki, M. B. Vasconcelos, K. S. Robinson, et al., "Mitochondrial Damage Activates the NLRP10 Inflammasome," *Nature Immunology* 24, no. 4 (2023): 595–603.

47. B. N. Martin, C. Wang, J. Willette-Brown, et al., "IKKα Negatively Regulates ASC-Dependent Inflammasome Activation," *Nature Communications* 5 (2014): 4977.

48. N. Kerur, V. Veettil Mohanan, N. Sharma-Walia, et al., "IFI16 Acts as a Nuclear Pathogen Sensor to Induce the Inflammasome in Response to Kaposi Sarcoma-Associated Herpesvirus Infection," *Cell Host & Microbe* 9, no. 5 (2011): 363–375.

49. R. Cao, B. Lin, H. He, et al., "CRM1 Mediates ASC Nuclear Export and Inflammasome Activation," *International Immunopharmacology* 153 (2025): 114503.

50. V. A. K. Rathinam, S. K. Vanaja, and K. A. Fitzgerald, "Regulation of Inflammasome Signaling," *Nature Immunology* 13, no. 4 (2012): 333–342.

51. H. Hara, K. Tsuchiya, I. Kawamura, et al., "Phosphorylation of the Adaptor ASC Acts as a Molecular Switch That Controls the Formation of Speck-Like Aggregates and Inflammasome Activity," *Nature Immunology* 14, no. 12 (2013): 1247–1255.

52. K. Guan, C. Wei, Z. Zheng, et al., "MAVS Promotes Inflammasome Activation by Targeting ASC for K63-Linked Ubiquitination via the E3 Ligase TRAF3," *Journal of Immunology* 194, no. 10 (2015): 4880–4890.

53. Y. C. Lin, D. Y. Huang, J. S. Wang, et al., "Syk Is Involved in NLRP3 Inflammasome-Mediated Caspase-1 Activation Through Adaptor ASC Phosphorylation and Enhanced Oligomerization," *Journal of Leukocyte Biology* 97, no. 5 (2015): 825–835.

54. T. Misawa, M. Takahama, T. Kozaki, et al., "Microtubule-Driven Spatial Arrangement of Mitochondria Promotes Activation of the NLRP3 Inflammasome," *Nature Immunology* 14, no. 5 (2013): 454–460.

55. R. Karki and T. D. Kanneganti, "Diverging Inflammasome Signals in Tumorigenesis and Potential Targeting," *Nature Reviews. Cancer* 19, no. 4 (2019): 197–214.

56. H. Zhang, L. Yang, Y. Liu, D. Wang, L. Shi, and C. Tian, "Integrative Multi-Omic Analysis of NLRP3 Inflammasome Dysregulation and Subtyping for Personalized Treatment in Acute Myeloid Leukemia," *Discover Oncology* 16, no. 1 (2025): 649.

57. A. Pagani, A. Nai, G. Corna, et al., "Low Hepcidin Accounts for the Proinflammatory Status Associated With Iron Deficiency," *Blood* 118, no. 3 (2011): 736–746.

58. M. Levy, H. Li, A. Dunbar, et al., "TMPRSS6 Antisense Oligonucleotide Therapy Reverses Inflammation in Jak2V617F Mutant Mice," *Blood* 144, no. Supplement 1 (2024): 8.

59. C. Zhong, R. Wang, M. Hua, et al., "NLRP3 Inflammasome Promotes the Progression of Acute Myeloid Leukemia via IL-1β Pathway," *Frontiers in Immunology* 12 (2021): 661939.

60. R. Ramanathan, Y. Xie, T. Badar, A. M. Zeidan, and S. A. Patel, "Contemporary Management Paradigms and Emerging Therapeutics for Myelodysplastic Syndromes/Neoplasms," *British Journal of Haematology* 206, no. 6 (2025): 1571–1581.

61. J. J. Rodriguez-Sevilla, V. Adema, K. S. Chien, et al., "The IL-1β Inhibitor Canakinumab in Previously Treated Lower-Risk Myelodysplastic Syndromes: A Phase 2 Clinical Trial," *Nature Communications* 15, no. 1 (2024): 9840.

62. E. S. Winer, A. Verma, S. Groepper, et al., "Preliminary Safety and Efficacy of Emavusertib (CA-4948) in Acute Myeloid Leukemia Patients With FLT3 Mutation," *Blood* 142, no. Supplement 1 (2023): 2924.

63. Y. Kawano, H. Kawano, M. W. LaMere, et al., "IL-1R1 and IL-18 Signals Regulate Mesenchymal Stromal Cells in an Aged Murine Model of Myelodysplastic Syndromes," *Blood* 145, no. 15 (2025): 1632–1644.

Supporting Information

Additional supporting information can be found online in the Supporting Information section. **Data S1:** Supporting Information.

10968652, 0, Downloaded from https://onlinelibrary.wiley.com/doi/10.1002/ajh.70391 by Alberto Martinez - NICE, National Institute for Health and Care Excellence , Wiley Online Library on [08/06/2026]. See the Terms and Conditions (https://onlinelibrary.wiley.com/terms-and-conditions) on Wiley Online Library for rules of use; OA articles are governed by the applicable Creative Commons License